Peer reviewed version of the manuscript published in final form at Advanced Healthcare Materials (205) DOI: 10.1002/adhm.201500677

Controlling Shear Stress in 3D Bioprinting is a Key Factor to Balance Printing Resolution and Stem Cell Integrity

Andreas Blaeser[1], Daniela Filipa Duarte Campos[1], Uta Puster[1], Walter Richtering[2], Molly M. Stevens[3], Horst Fischer[1*]

1. Department of Dental Materials and Biomaterials Research, RWTH Aachen University Hospital, Aachen, Germany
2. Institute of Physical Chemistry, RWTH Aachen University, Aachen, Germany
3. Department of Materials, Department of Bioengineering and Institute of Biomedical Engineering, Imperial College London, London, UK

*E-mail: hfischer@ukaachen.de

Abstract

A microvalve-based bioprinting system for the manufacturing of high-resolution, multimaterial 3D-structures is reported. Applying a straightforward fluid-dynamics model, the shear stress at the nozzle site can precisely be controlled. Using this system, a broad study on how cell viability and proliferation potential are affected by different levels of shear stress is conducted. Complex, multimaterial 3D structures are printed with high resolution. This work pioneers the investigation of shear stress-induced cell damage in 3D bioprinting and might help to comprehend and improve the outcome of cell-printing studies in the future.

Bioprinting is an emerging tissue engineering (TE)[1-4] discipline that pursues the goal of generating viable tissue constructs using additive manufacturing technologies. Cell-laden hydrogels are printed layer-by-layer according to a predefined, 3D model.[5-7] The hydrogel-cell suspension is usually printed as a liquid solution (sol-state) and undergoes gelling, chemically or physically triggered, after the dispensing process. While traditional TE techniques, such as hydrogel casting,[8] involve three key elements—cells, scaffolds, and growth factors[9]—the dispensing process in bioprinting represents a

fourth. According to the latter, most bioprinting technologies can be classified into three categories[6]: robotic dispensing,[10-14] laser-based bioprinting (e.g., LIFT),[15-17] and inkjet printing.[18-22] LIFT and inkjet represent contactless printing techniques where discrete drops are dispensed one-by-one. In contrast, robotic dispensing techniques deposit continuous lines of hydrogel alongside a distinct pathway. The potential to deposit different cell types and biomaterials with high spatial resolution is both a blessing and a curse. It enables the generation of complex, multicellular tissue structures (e.g., vascularized tissue constructs)[12, 23, 24] that cannot be created otherwise. On the other hand, the dispensing process involves mechanical stress, thermal stress, or a combination of both and ultimately affects cell behavior.[25-28]

Shear stress is of special interest in bioprinting. It is inevitable in any dispensing process and therefore has to be considered in all printing methods. The level of shear stress is directly influenced by different printing parameters, such as nozzle diameter, printing pressure, and viscosity of the dispensing medium.[25, 26] Moreover, shear stress plays a decisive role in cell biology,[29, 30] e.g., in cell signaling and protein expression.[31-33] For instance, it is reported that shear stress promotes maturation of megakaryocytes.[34] Moderate shear stress was found to have an influence on stem cell differentiation.[35] Excessive shear stress, in contrast, even dispatches cells by disrupting the membrane. These phenomena are even more crucial in bioprinting processes, where hydrogels of high viscosity and small nozzles are applied in an attempt to improve the final printing resolution. Here, we show that both hydrogel viscosity and nozzle size directly affect shear stress. To prevent adverse cell response and printing-related cell death, it is essential to control the shear stress level, identify its most important drivers, and study the cell response upon different stress levels. We hypothesize that regulating shear stress and elucidating its impact would be of great use in balancing cell integrity and printing resolution.

We present a microvalve-based bioprinting system for the manufacturing of high resolution, multi-material 3D structures (Scheme 1A). Applying a straightforward fluid-dynamics model, we were able

to precisely control shear stress at the nozzle site, which could be adjusted by varying the printing pressure, hydrogel viscosity, and the nozzle diameter. Using this system, we conducted a broad study on how cell viability and proliferation potential are affected by different levels of shear stress (Scheme 1B). Generating complex, multi-material 3D-structures, we demonstrate that high-resolution printing at moderate, cell-friendly nozzle shear stress are not mutually exclusive.

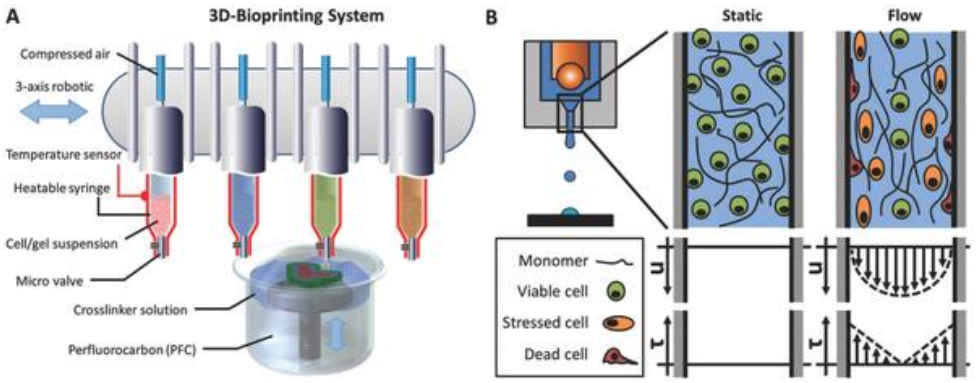

Scheme 1. *A) Concept of the 3D-bioprinting system with bi-phasic support liquid for the manufacturing of thin-walled, multilayered hydrogel structures. B) Schematic illustration of the velocity and shear stress distribution as well as the stress impinged on cells inside a bioprinter nozzle.*

The printer used throughout this study comprised four microvalve-based print heads, each individually controllable and heatable, mounted to a three-axis robotic system (Figure S1, Supporting Information). A metal stage that could be lowered into a container filled with a bi-phasic support liquid—perfluorocarbon (PFC) and an aqueous crosslinker solution— was used as a printing platform that allowed for the manufacturing of macroscopic, multi-layered 3D structures (Figure S1, Supporting Information). The presented printing system dispenses single drops of cell-hydrogel suspension by jetting using electromagnetic microvalves. Thus, cells are primarily exposed to mechanical stress in the form of shear stress. To describe the shear stress condition in the nozzle of the valve, we developed a fluid dynamics model for transient flow of non-Newtonian fluids (hydrogels) based on the Bernoulli equation for unsteady flow: Equation (1), the law of Hagen–Poisseuille: Equation (2), and the

Ostwald–de Waele relationship (or Power-law): Equation (3).[36] Nomenclature of all symbols appearing in the listed equations can be found in Table S5 (Supporting Information).

$$p_n + \rho g h_n + \rho \frac{1}{2} w_n^2 = p_{n+1} + \rho g h_{n+1} + \frac{1}{2} \rho w_{n+1}^2 + \rho \int_0^{Sn} \frac{\partial w}{\partial t} ds + \Delta p(w,\eta) \quad (1)$$

$$\Delta p(w,\eta) = 8 \frac{\dot{V} \eta s}{\pi r^4} \quad (2)$$

$$\eta = K \left(\frac{\delta w}{\delta r} \right)^{n-1} \quad (3)$$

Equations (1), (2) and (3) can be transformed into a nonlinear, first-order differential equation, Equation (4), that describes the hydrogel flow through the microvalve considering wall-friction and intrinsic shear stress (Supporting Information).

$$\frac{\partial w}{\partial t} = \frac{1}{\rho s} \left(p + \rho g h - \frac{1}{2} \rho w^2 - \frac{4}{d} w^n K \left[\frac{2\left(\frac{1}{n} + 3\right)}{d} \right]^n \right) \quad (4)$$

Solving Equation (4) numerically, we were able to calculate the average drop speed (*w*), the drop volume () and the shear stress occurring inside the valve (*τ*) for different nozzle dimensions (diameter *d*, length *s*) and hydrogels of different viscosities (consistency index *K*, power-law exponent *n*) at a given gating time (*t*), Tables S1–S4 and Figures S2–S5 (Supporting Information).

We selected alginate, a shear-thinning hydrogel that is widely used in tissue engineering applications,[37, 38] as model fluid for the shear stress study. The viscosity as well as the power-law constants (*K* and *n*) of three differently concentrated alginate solutions (0.5, 1.0, 1.5 wt/v%) were measured using a dynamic shear rheometer (Figure 1A–C and Table 1). The viscosity was measured for pure alginate solution (without cells) as well as for alginate suspended with 1 and 10 million cells

per milliliter, respectively. Interestingly, cell-laden alginate solutions exhibited a lower viscosity than the cell-free one (Figure 1A). This effect can be attributed to the addition of cell-culture medium, which influences the pH-value and the ionic-strength and was not present in the pure alginate sample. However, with increasing cell number (from 1 m to 10 m) the flow consistency index (*K*) increased while the flow behavior index (*n*) diminished (Table 1). Thus, the presence of cells has an effect on the rheology of hydrogels. Higher cell numbers increase viscosity and amplify the shear thinning effect.

Table 1. *Rheological characterization of cell-free and cell-laden alginate solutions. The power law constants, flow consistency index (K), and flow behavior index (n), of differently concentrated alginate solutions are listed.*

	0.5 wt/v% alginate		**1.0 wt/v% alginate**		**1.5 wt/v% alginate**	
	n	*K* [Pa s^n]	*N*	*K* [Pa s^n]	*n*	*K* [Pa s^n]
No cells	0.977	0.032	0.895	0.119	0.840	0.346
1 × 10^6 cells mL^{-1}	0.986	0.020	0.963	0.066	0.913	0.158
10 × 10^6 cells mL^{-1}	0.940	0.029	0.942	0.080	0.910	0.161

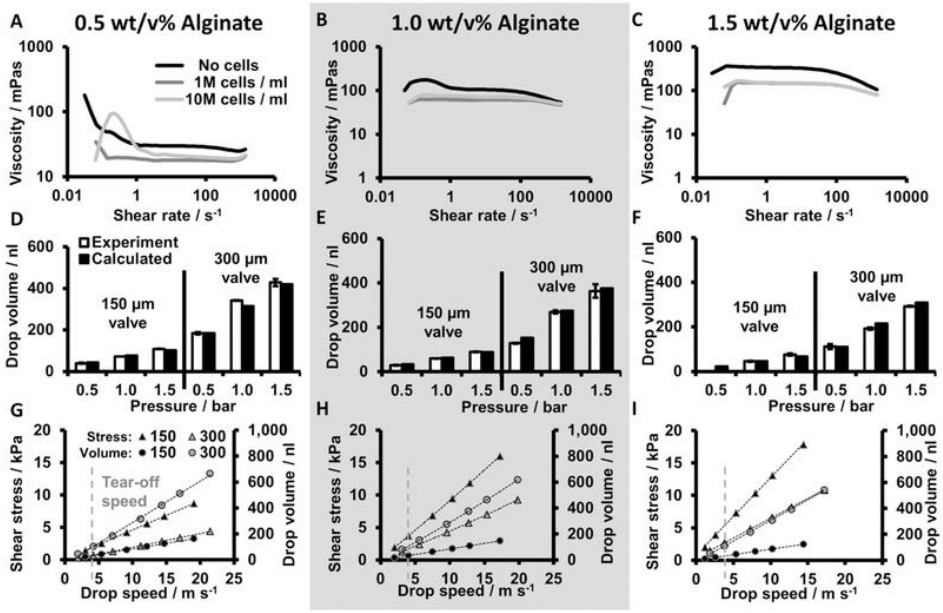

Figure 1. *A–C) Rheological characterization of differently concentrated alginate hydrogels with and without cells. The humps in the viscosity curves at low shear rates represent measurement artifacts,*

which were not considered in the evaluation later on. D–F) Validation of the fluid dynamic model by comparing the estimated drop volume with experimentally derived values for three different alginate gels, different valve sizes (150 and 300 µm) and pressures (0.5–1.5 bar). Comparison of shear stress (Δ) and drop volume (o) of two valve sizes (150 µm and 300 µm) at different drop speeds (0–25 m s^{-1}). G–I) The minimal speed required to tear the drop off the nozzle (4 m s^{-1}) is indicated with a dotted line.

To validate the fluid dynamic model, the calculated drop volume was compared with experimentally derived values (Figure 1D–F). For a broad range of printing pressures (0.5–1.5 bar), two different nozzle diameters (150 µm and 300 µm) as well as the tested alginate concentrations (0.5–1.5 wt/v%) the model closely matched the measured results. The theoretical drop speed at the nozzle exit was calculated to be in a range from 1 to 20 m s^{-1} (Table S4, Supporting Information). The minimal speed required to actually fire a single drop was found to be 3.8 m s^{-1}. For velocities below the tear-off threshold, hydrogel only accumulated at the nozzle tip but no single drops could be formed. Both the estimated drop speed range and the assessed tear-off speed were in accordance with previously published studies on drop kinetics of inkjet printers.[39-41] The calculated average shear stress in the nozzle was found to be in a range from 0.7 to 18 kPa. To optimize the printing process in terms of shear stress and printing resolution, the nozzle shear stress as well as the drop volume is plotted against the drop speed, Figure 1G–I. The experimentally derived tear-off speed is marked by a vertical line. It marks the minimal drop volume and nozzle shear stress that can be achieved by a specific valve (150 µm or 300 µm). The results indicate a strong influence of the nozzle size on both shear stress and drop volume. Using bigger valves results in lower shear stress, while the drop volume rises. For instance, reducing the nozzle diameter from 300 to 150 µm, while printing solutions with a relatively low concentration of alginate (0.5 wt/v%) at a drop speed close to the tear-off threshold (4 m s^{-1}), resulted in a 2.8-fold gain in shear stress (from 0.7 to 1.9 kPa). At the same time, drop volume is three times decreased (from 97 to 32 nL). Interestingly, the shear stress difference between the two nozzles diminishes with increasing hydrogel viscosity while the gap in the drop volumes rises. For solutions with a relatively higher concentration of alginate (1.5 wt/v%), the shear stress rises only by factor 2.0

(from 2.8 to 5.6 kPa), when the nozzle size is reduced, whereas the drop volume is 3.4 times higher (from 34 to 116 nL). To answer the question of whether it is reasonable to improve printing resolution by accepting higher shear stress, it is essential to evaluate the impact of shear stress on living cells. We hypothesized that printing-induced shear stress does not only have an immediate impact on cell viability, for instance by damaging the cell membrane, but in the long run also alters the behavior of cells that survived the printing process. We analyzed the viability of cells (L929, mouse fibroblasts) exposed to a wide range of nozzle shear stress (0.7–18 kPa) immediately after printing (Figure 2A). According to the applied nozzle shear stress, we classified the results into three groups (<5 kPa, 5–10 kPa, >10 kPa, Figure 2B). Viability, and hence the membrane integrity, of cells exposed to low rates of shear stress (<5 kPa) was almost unaffected by the printing process (96% cell viability). In contrast, the average cell viability significantly decreased for the two higher shear stress groups (91% and 76% cell viability). The results confirm the hypothesis that printing related cell damage is directly associated with the applied nozzle shear stress. Furthermore, the observations indicate that below a critical shear stress level cells can be dispensed without impairment.

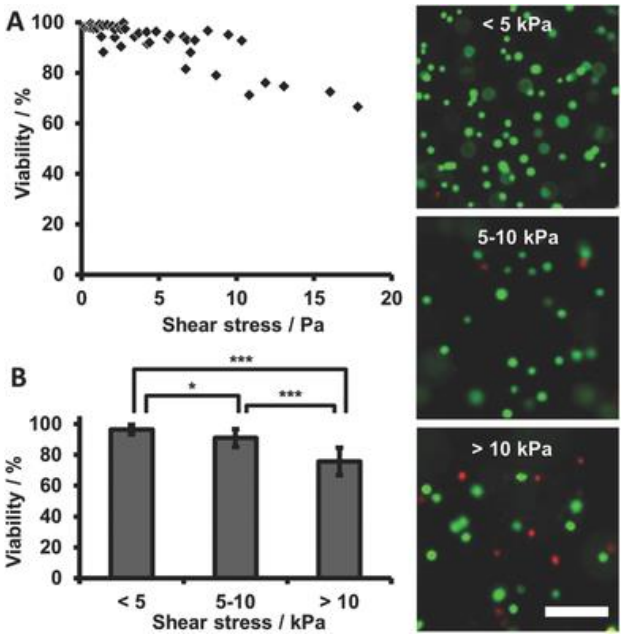

Figure 2. *Screening study to investigate the impact of shear stress on post-printing cell viability using L929 mouse fibroblasts. A) In total 44 experiments with shear stress ranging from 0 to 20 kPa were*

conducted. B) Cell viability was assessed immediately after printing (day 0) using live/dead staining assay. The results were summarized in three groups (<5 kPa, 5–10 kPa, and > 10 kPa). The graphs illustrate mean ± SD. Significance levels were p *< 0.005 (***),* p *< 0.05 (*). On the right side, examples of pictures from the microscopic analysis of the post-printing cell viability are shown (scale bar represents 100 µm).*

Next, we sought to investigate the short-term and possible long-term effects of printing induced shear stress on primary human mesenchymal stem cells (hMSC). We printed hMSC from five independent donors (n = 5) at three different shear stress levels (4, 9, and 18 kPa) and recorded cell viability as well as proliferation potential for up to 7 d after printing (Figure 3). With increasing shear stress, we found that post-printing cell viability (day zero) significantly decreased from 94% (4 kPa) to 92% (9 kPa), and 86% (18 kPa), respectively, which is in accordance with the findings using mouse fibroblasts (Figure 3A,C,D) discusses above. After 7 d of culture, cell viability increased to 95%–97% and no significant differences between the printed groups could be found. However, viability of printed cells was slightly but significantly lower than in the non-printed control group. In a second study, we took a closer look to the proliferation potential of printed hMSC using a quantitative cell proliferation assay (Figure 3B). The number of cells at a given time point is expressed in relative fluorescence units (RFUs). Growth of cells exposed to low shear-stress (<5 kPa) did not seem to be affected by the printing process. Though cell numbers were slightly lower than the controls, the differences were not significant at any time point. In contrast, cell growth was strongly affected by higher levels of shear-stress (5–10 kPa and >10 kPa). Cell numbers were significantly lower than in the control group and after 4 d of incubation even lower than the first group (<5 kPa). Nonetheless, all samples showed a significant gain in the number of cells from day one to day seven. Furthermore, the proliferation rate, i.e., the ratio between the numbers of cells measured at day seven and day one, of cells printed at low (<5 kPa) and medium (5–10 kPa) shear stress was even higher than the controls. In both printed groups, the number of cells showed a 2.8-fold increase, while the control increased by the factor 2.4. Yet, cells printed at high shear stress (>10 kPa) only proliferated by the factor 1.9. These results indicate that moderate levels

of shear stress might even stimulate cell proliferation, whereas this effect is reversed when a certain stress threshold is exceeded. Similar findings have already been published in the past, even though cells were exposed to much lower doses of shear stress over prolonged periods.[42-45] Riddle et al. discovered that moderate shear stress elevates the intracellular calcium concentration and increases hMSC proliferation.[45] However, to elucidate this phenomenon additional mechanobiological studies with a focus on intracellular mechanisms in response to shear stress should be conducted.

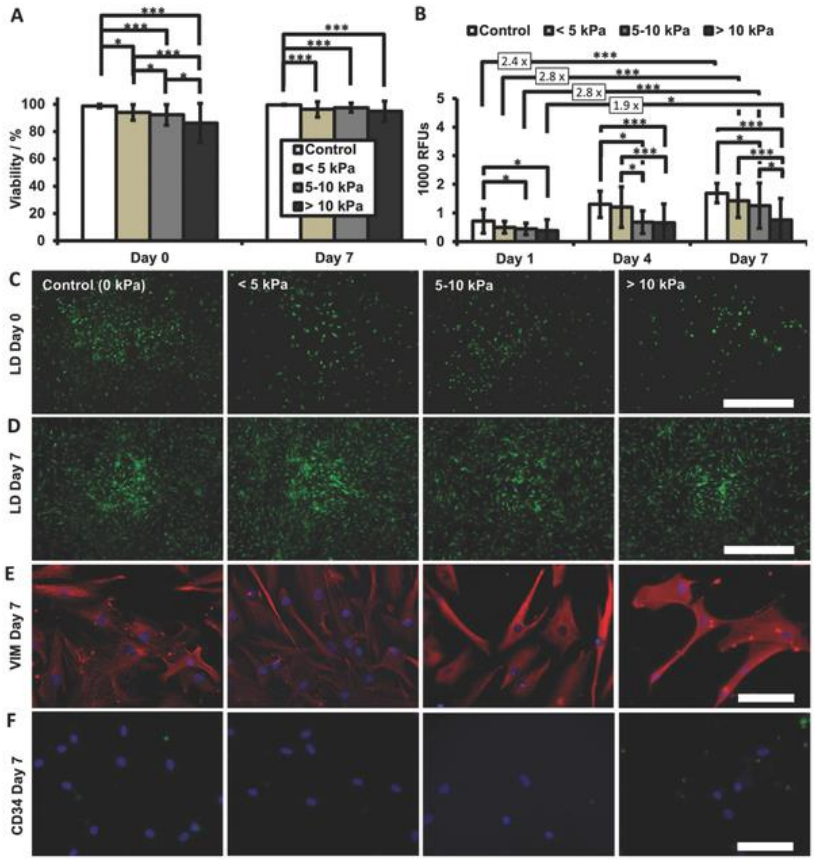

Figure 3. *Short-term and long-term impact of different shear stress levels (<5 kPa, 5–10 kPa, and >10 kPa) on A) human mesenchymal stem cell viability, B–D) proliferation, and E,F) mesenchymal marker expression. The study was conducted with five independent donors (n = 5) for up to 7 d. The graphs A and B show a strong impact of the level of shear stress on cell viability and proliferation potential. The graphs illustrate mean ± SD. Significance levels were p < 0.005 (***), p < 0.05 (*). The images C and D depict cell viability and growth over time (scale bar in C and D represent 1 mm, respectively). E) The mesenchymal marker vimentin stained positive, whereas F) the hematopoetic marker CD34 stained*

negative, proving that the MSC phenotype remained unaltered after printing (scale bar in E and F represents 100 µm, respectively).

In order to determine if the phenotype of hMSC was altered by shear stress we stained for typical mesenchymal markers by immunocytochemistry (Figure 3E,F). Staining was done for vimentin, an intermediate filament mesenchymal marker, and for the endothelial marker CD34, which was expected to be negative in hMSC. The results indicate that the mesenchymal phenotype of cells remained unaffected at all tested shear stress levels for at least 7 d after printing. The findings of our study show that short-time exposure to high levels of shear stress does not only affect cell viability immediately after printing but can also induce long-term alterations in the proliferation potential of cells that survived the dispensing process. However, even when exposed to high levels of shear stress, cells did not display phenotypic alterations. Cells that were exposed to comparably low levels of shear stress (<5 kPa) exhibited neither short-term nor long-term impairments. These findings suggest, that below a specific shear stress threshold, cells can be printed without side effects. For the tested cell types (L929 and hMSC), we found this threshold to be around 5 kPa. In comparison, the physiological shear stress that occurs in blood vessels measures only a thousandth of that value (7 Pa).[46]

As a final step, we demonstrate that high-resolution bioprinting of viscous materials is possible at a low shear stress level. Models of arbitrary hollow structures were generated with computer aided design (CAD) software, transformed into a multi-layered drop model using a custom designed algorithm (Figures S6–S8, Supporting Information) and printed, subsequently, in an alginate hydrogel (0.5 wt/v%) and utilizing a 150 µm micro valve (Figure 4A–C). The printing pressure was adjusted to 0.5 bar resulting in a drop speed of 5.4 m s^{-1}, which was just above the tear-off speed necessary for drop generation. Thus, both the drop volume (44 nL) as well as the nozzle shear stress (2.5 kPa) could be reduced to a minimum. Applying these settings, we were able to print multi-layered, hollow alginate structures with a minimal wall thickness measuring a few hundred micrometers (Figure 4D–F). The structures, which measured up to 1.5 cm in height, could be generated in less than 15 min. To

facilitate the manufacturing process, a bi-phasic support liquid system based on perfluorocarbon (PFC) and a crosslinker solution ($CaCl_2$) in combination with a solid, fugitive material composed of gelatin and agarose were applied (Figure S1, Supporting Information). Besides its advantage in mechanically stabilizing the printed structure, the supporting liquid prevents the hydrogel from drying out. The fugitive material was designed to gel in a thermally reversible manner and a sol–gel transition was observed at 37 °C. The fugitive material (illustrated as white drops) determined the final shape of the printed structure and provided mechanical support. It was removed after printing by incubating the generated structures at 37 °C for 12 h in cell culture medium or distilled water leaving a perfusable alginate shell (Video S1, Supporting Information).

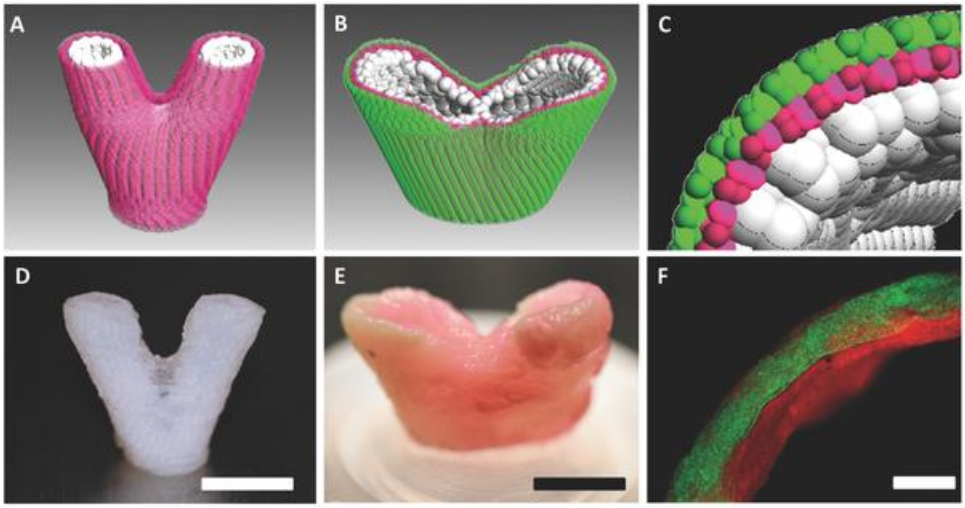

Figure 4. *A–C) Thin-walled, multilayered 3D structures were modeled with computer-aided design software, sliced with a custom-designed algorithm, and finally printed using the 3D-bioprinting system with bi-phasic support liquid (D and E, scale bar represent 5 mm, respectively). A–C) The white drops define the fugitive material composed of agarose and gelatin. Red and green drops mark the alginate shell. The F) microscopic picture shows a higher magnification of the 3D structure, which is displayed in E (scale bar represents 500 µm).*

In summary, we showed that profound knowledge about fluid-dynamics and shear stress associated with the drop formation process are crucial to optimize both printing resolution and cell response in

drop-on-demand 3D-bioprinting. We identified three key factors that influence drop formation, namely printing pressure, hydrogel viscosity, and nozzle size and investigated their impact on shear stress as well as printing resolution. We showed that short-time exposure to high levels of shear stress affects cells immediately and furthermore can induce long-term alterations in the proliferation potential of the cells that have survived the dispensing process. Our findings suggest that below a specific shear stress threshold cells can be printed without side effects. Finally, we showed that the printing process can be tuned to generate multilayered, hydrogel structures with high resolution at a low shear stress level. This work pioneers the investigation of shear stress-induced cell damage in 3D-bioprinting and might help to comprehend and improve the outcome of cell-printing studies in the future. Even though the presented data are specific for microvalve-based bioprinting and thus cannot be directly applied to other hydrogel precursor delivery methods, such as microextrusion, the results of the cell study are of great value for other biofabrication techniques inasmuch as they give a clue on how cells generally respond to short-time exposure to moderate and high levels of shear stress. Furthermore, the mathematical analysis presented in this work can easily be adapted to the continuous extrusion of hydrogels, which represents steady flow and hence can be described by a much simpler fluid dynamics model. However, in valve-based printing systems, where cells are ejected in a sudden burst, controlling shear stress is more critical and thus more important than in other biofabrication techniques.

Experimental Section

Hydrogel Preparation: We prepared two different types of hydrogels, alginate, which was used as model gel in all experiments, and additionally a fugitive material composed of agarose and gelatin, which was used as a solid support in the 3D bioprinting study. We prepared five different alginate concentrations (0.5, 1.0, 1.5, 2.0, and 3.0 wt/v%) by dissolving 0.005, 0.010, 0.015, 0.020, and 0.030 g mL^{-1} alginic acid sodium salt from brown algae (alginic acid sodium salt from brown algae, 71238, Sigma, St. Louis, MO, USA) in deionized 0.2 µm sterile-filtered water. To achieve a homogeneous

distribution, the alginate solution was mixed for 12 h on a rolling mill. All studies related to pure alginate were conducted with gel derived from the 0.5, 1.0, and 1.5 wt/v% stock solutions. For the cell studies, alginate stock solutions (1.0, 2.0, and 3.0 wt/v%) were mixed 1:1 with equal volumes of cells suspended in culture medium resulting in a final concentration of 0.5, 1.0, and 1.5 wt/v% alginate with 1×10^6 and 10×10^6 cells mL^{-1}, respectively. The fugitive material was composed of 0.5 wt/v% agarose and 5.0 wt/v% gelatin. Stock solution of 1.0 wt/v% agarose was prepared by mixing 0.01 g mL^{-1} agarose (low gelling agarose A9414; Sigma, St. Louis, MO) with tap water. The agarose solution was subsequently autoclaved at 121 °C for 15 min. Stock solution of 10.0 wt/v% gelatin was prepared by mixing 0.10 g mL^{-1} gelatin (gelatin type A, G2500, Sigma, St Louis, MO, USA) with deionized sterile-filtered water. After swelling for 10 min, the gelatin was melted in a water bath at 37 °C. Agarose and gelatin stock solutions were mixed 1:1. For the 3D-bioprinting experiment, both alginate and fugitive material were stained using 0.1 v/v% of differently colored phosphorescent dyes (Neon Nights Glow Paint Phosphorescent, Individual UG, Langenfeld, Germany).

Rheological Characterization: The viscosity of alginate hydrogels was characterized using a rotary rheometer (Kinexus, Malvern Instruments, Worcestershire, UK) with a 4° cone and plate geometry. Shear stress and viscosity were measured for shear rates from 0.01 to 1500 s^{-1} and at different temperatures (20 °C, 30 °C, and 40 °C). The power-law constants (*K* and *n*) were derived from the intercept and slope of the shear stress to shear rate graphs (Figure S3, Supporting Information).

Validation of the Fluid Dynamic Model: A straight-forward fluid dynamics model describing transient flow of Newtonian and non-Newtonian fluids through a microvalve was developed based on the Bernoulli equation for unsteady flow: Equation (1), the law of Hagen–Poisseuille: Equation (2), and the Ostwald–de Waele relationship (or Power-law): Equation (3). Based on Equations (1), (2), (3) and the valve geometry, a nonlinear first-order differential equation describing the hydrogel flow through the valve was derived (Equation (4)), Supporting Information). The model was adapted to the geometry of SMLD 300G microvalves (Fritz Gyger, Gwatt, Switzerland) and experimentally validated. The valve

geometry was simplified and considered as three pipe sections with different lengths and different cross-sections (Supporting Information). Valves with two different nozzle diameters (150 and 300 µm) were tested. Apart from the nozzle, the valves were identical. To validate the model, we predicted the drop volume for differently concentrated alginates (0.5–1.5 wt/v%), over a broad range of printing pressures (0.5–1.5 bar) and both valve types (150 and 300 µm) at a fixed gating time (500 µs). The calculated results were compared to experimentally derived values. For each set of printing parameters, 1000 drops were printed into a glass vessel, their weight was measured and divided by 1000. The average drop volume was calculated using the density of water (1000 kg m^{-3}). Each experiment was repeated three times.

Isolation of Human Mesenchymal Stem Cells: Human mesenchymal stem cells (hMSC) were isolated from the femoral heads of five independent donors as described previously.[47, 48] The spongiosa was flushed with hMSC medium using a 22G-needle. The resulting cell suspension was centrifuged and seeded in T75 flasks for 24 h. Hematopoietic nonadherent cells were washed out by the exchange of the hMSC medium. Remaining cells, which were adherent, were cultured and expanded for two to four passages in hMSC growth medium (Mesenpan; PAN Biotech, Aidenbach, Germany) containing 2 v/v% fetal calf serum (FCS) and 1 v/v% penicillin/streptomycin (Gibco, Life Technologies, Carlsbad, CA, USA).

Shear Stress-Related Cell Study: L929 mouse fibroblasts (CCL-1, American Type Culture Collection) were cultured in low-glucose DMEM supplemented with 10 v/v% FCS and 0.4 v/v% gentamycin (10 mg mL^{-1}). Cells were re-suspended in alginate resulting in a final cell density of 1×10^6 cells per milliliter. Drops of 10 µL cell hydrogel suspension were printed onto a microscopy glass slide at different pressures (0.5–3.0 bar) using both valve types (150 and 300 µm). Cell viability was assessed immediately after printing applying vital-fluorescence-staining using an inverted microscope (DMI6000B, Leica Microsystems, Wetzlar, Germany). The staining solution contained 0.083 mg mL^{-1} propidium iodide (P4170-10116, Sigma–Aldrich, St. Louis, USA) and 0.083 mg mL^{-1} fluorescein

diacetate (F7378-10G, Sigma–Aldrich, St. Louis, MO, USA) in Ringer's solution. Each experiment was repeated three times. The number of living and dead cells was counted using ImageJ. Cell viability, i.e., the ratio between living and dead cells, was plotted against the shear stress, which was calculated for each set of printing parameters using the fluid dynamics model.

Human mesenchymal stem cells were mixed with alginate resulting in a final cell density of 1×10^6 cells per milliliter. For viability and immunofluorescence studies, 10 µL of hMSC-laden alginate was printed drop-by-drop onto circular glass slides inside a 24-well plate resulting in a seeding density of 5×10^3 cells cm^{-2}. After printing, the alginate-cell drops were resuspended in cell-culture medium in order to dilute the alginate and let the cells adhere and grow on the glass slide. Viability of cells growing on the glass was assessed immediately and 7 d after printing as described for L929 fibroblasts. For each donor, three independently printed samples were tested. For the immunofluorescence study, cells were washed with PBS and fixated with 4 v/v% paraformaldehyde for 15 min. Primary antibodies vimentin (1:200, Sigma, Sigma–Aldrich, St. Louis, MO, USA) and CD-34 (1:250, Abcam, Cambridge, UK), were applied for 45 min. Thereafter, secondary antibodies (1:2000 Alexa Fluor 488/555, rabbit/mouse, Life Technologies, Carlsbad, CA, USA) were added. The samples were imaged within 24 h after the staining. To measure the proliferation potential 1.4 µL MSC-laden alginate were printed on circular glass slides inside a 96-well plate, resuspended with 98 µL medium, and cultured for up to 7 d. For each donor and each time point (1, 4, and 7 d), six independently printed samples were analyzed. The growth potential was quantified as described previously [48] using a proliferation assay (CellTiter-Blue, Promega, Madison, WI, USA). Briefly, 25 microliters of CellTiter-Blue were mixed with 100 µL medium, added to each well-plate and incubated at 37 °C for 1 h. The absorbance was read at 560 nm/590 nm (excitation/emission wavelength) using a plate reader (InfinitiM200, Tecan, Männedorf, Switzerland). For all experiments (viability, immunofluorescence, and proliferation) nonprinted hMSC cultured on glass slides were used as positive controls.

3D Bioprinting of Multilayered Alginate Structures: All experiments, including shear stress studies and printing tests, were conducted with a custom-built 3D-bioprinter (Figure S1, Supporting Information). The printer comprised four microvalve (Fritz Gyger, Gwatt, Switzerland)-based print heads, each individually controllable and heatable, mounted to a three-axis robotic system (Isel, Eichenzell, Germany). The printing pressure could be varied from 0 to 3 bar. The print head enabled quick exchange of the attached micro valves to change between the small (150 µm) and big (300 µm) nozzle. A titan stage that could be lowered into a container filled with a bi-phasic support liquid—perfluorocarbon (PFC, Fluorinert Electronic Liquids FC-43, 3M, St. Paul, MN, USA) and 50 mg mL^{-1} calcium chloride solution—was used as a printing platform. Due to the difference in density, the aqueous $CaCl_2$ solution floats on the top of the PFC, building a thin liquid layer, wherein the crosslinking of the printed alginate occurred. With every successfully printed layer, the titan stage was lowered into the bi-phasic support liquid. To ensure that the lastly printed hydrogel layer would not be submerged, stage lowering was adjusted to the level of the crosslinker solution. For printing of multilayered alginate structures, the bi-phasic support liquid was cooled down to 10 °C using a cooling aggregate (TC45-F, Peter Huber Kältemaschinenbau, Offenburg, Germany). The print head carrying the agarose–gelatin fugitive material was heated up to 50 °C and the printing pressure was set to 1.5 bar. The two print heads carrying the alginate hydrogel (0.5 wt/v%) worked at room temperature (20 °C) at a pressure of 0.5 bar. All 3D bioprinting experiments were conducted using the 150 µm nozzle. After printing the fugitive material was liquefied by keeping the samples in an incubator at 37 °C for 12 h. The fugitive material could be flushed out with distilled water or PBS thereafter.

Acknowledgements

The authors are grateful to Roswitha Davtalab and Galen Kreutzberg for their help conducting the stem cell study. Special thanks go to Azher Sultan, Darius Hinüber, and Michael Weber for their support in building up the 3D bioprinting system, and Lukas Florea as well as Tong Zhao for their contribution to the slicing algorithm (all Department of Dental Materials and Biomaterials Research, RWTH Aachen University Hospital). In addition, the authors thank Fiete Dierkes and Ralph Klemp from the Institute of Physical Chemistry, RWTH Aachen University for their help in the rheological characterization of alginate solutions.

References

1. R. Langer, J. P. Vacanti, Science 1993, 260, 920.
2. E. S. Place, N. D. Evans, M. M. Stevens, Nat. Mater. 2009, 8, 457.
3. P. Zorlutuna, N. Annabi, G. Camci-Unal, M. Nikkhah, J. M. Cha, J. W. Nichol, A. Manbachi, H. Bae, S. Chen, A. Khademhosseini, Adv. Mater. 2012, 24, 1782.
4. R. D. Abbott, D. L. Kaplan, Trends Biotechnol. 2015, 33, 401.
5. B. Derby, Science 2012, 338, 921.
6. S. V Murphy, A. Atala, Nat. Biotechnol. 2014, 32, 773.
7. L. E. Bertassoni, M. Cecconi, V. Manoharan, M. Nikkhah, J. Hjortnaes, A. L. Cristino, G. Barabaschi, D. Demarchi, M. R. Dokmeci, Y. Yang, A. Khademhosseini, Lab Chip 2014, 14, 2202.
8. G. Forgacs, Nat. Mater. 2012, 11, 746.
9. J. Malda, J. Visser, F. P. Melchels, T. Jüngst, W. E. Hennink, W. J. Dhert, J. Groll, D. W. Hutmacher, Adv. Mater. 2013, 25, 5011.
10. W. Wu, A. DeConinck, J. Lewis, Adv. Mater. 2011, 23, H178.
11. A. Agrawal, N. Rahbar, P. D. Calvert, Acta Biomater. 2013, 9, 5313.
12. D. B. Kolesky, R. L. Truby, S. Gladman, T. Busbee, K. Homan, J. Lewis, Adv. Mater. 2014, 26, 2966.

13. K. Schacht, T. Jüngst, M. Schweinlin, A. Ewald, J. Groll, T. Scheibel, Angew. Chem. Int. Ed. 2015, 54, 1.
14. S. Mishra, F. J. Scarano, P. Calvert, J. Biomed. Mater. Res. A 2015, 103, 3237.
15. B. Guillotin, A. Souquet, S. Catros, M. Duocastella, B. Pippenger, S. Bellance, R. Bareille, M. Rémy, L. Bordenave, J. Amédée, F. Guillemot, Biomaterials 2010, 31, 7250.
16. M. Ali, E. Pages, A. Ducom, A. Fontaine, F. Guillemot, Biofabrication 2014, 6, 045001.
17. Z. Zhang, R. Xiong, R. Mei, Y. Huang, D. B. Chrisey, Langmuir 2015, 31, 6447.
18. P. Calvert, Science 2007, 318, 208.
19. W. Lee, V. Lee, S. Polio, P. Keegan, J.-H. Lee, K. Fischer, J.-K. Park, S.-S. Yoo, Biotechnol. Bioeng. 2010, 105, 1178.
20. H. Tao, B. Marelli, M. Yang, B. An, S. Onses, J. A. Rogers, D. L. Kaplan, F. G. Omenetto, Adv. Mater. 2015, 29, 4245.
21. G. Gao, T. Yonezawa, K. Hubbell, G. Dai, X. Cui, Biotechnol. J. 2015, 10, 1568.
22. K. Christensen, C. Xu, W. Chai, Z. Zhang, J. Fu, Y. Huang, Biotechnol. Bioeng. 2015, 112, 1047.
23. V. K. Lee, D. Y. Kim, H. Ngo, Y. Lee, L. Seo, S.-S. Yoo, P. Vincent, G. Dai, Biomaterials 2014, 35, 8092.
24. V. K. Lee, A. M. Lanzi, N. Haygan, S.-S. Yoo, P. Vincent, G. Dai, Cell. Mol. Bioeng. 2014, 7, 460.
25. R. Chang, J. Nam, W. Sun, Tissue Eng. Part A 2008, 14, 41.
26. K. Nair, M. Gandhi, S. Khalil, K. C. Yan, M. Marcolongo, K. Barbee, W. Sun, Biotechnol. J. 2009, 4, 1168.
27. X. Cui, D. Dean, Z. M. Ruggeri, T. Boland, Biotechnol. Bioeng. 2010, 106, 963.
28. J. Hendriks, C. Willem Visser, S. Henke, J. Leijten, D. B. F. Saris, C. Sun, D. Lohse, M. Karperien, Sci. Rep. 2015, 5, 11304.
29. K. H. K. Wong, J. M. Chan, R. D. Kamm, J. Tien, Annu. Rev. Biomed. Eng. 2012, 14, 205.
30. Z. M. Ruggeri, J. N. Orje, R. Habermann, A. B. Federici, A. J. Reininger, Blood 2015, 108, 1903.
31. S. Chien, Annu. Rev. Biomed. Eng. 2008, 36, 554.

32. P. Galie, D.-H. T. Nguyen, C. K. Choi, D. M. Cohen, P. Janmey, C. S. Chen, Proc. Natl. Acad. Sci. USA 2014, 111, 7968.
33. R. Busch, A. Strohbach, M. Pennewitz, F. Lorenz, M. Bahls, M. C. Busch, S. B. Felix, Cell Signal. 2015, 27, 1286.
34. J. Jiang, D. S. Woulfe, E. T. Papoutsakis, Blood 2015, 124, 2094.
35. C. M. F. Potter, K. H. Lao, L. Zeng, Q. Xu, Arterioscler., Thromb., Vasc. Biol. 2014, 34, 2184.
36. W. Bohl, W. Elmendorf, Technische Strömungslehre, Vogel Buchverlag, Würzburg, Germany, 2005.
37. M. M. Stevens, R. P. Marini, D. Schaefer, J. Aronson, R. Langer, V. P. Shastri, Proc. Natl. Acad. Sci. USA 2005, 102, 11450.
38. M. S. Hahn, B. Teply, M. M. Stevens, S. M. Zeitels, R. Langer, Biomaterials 2006, 27, 1104.
39. G. L. Fillmore, IEEE Trans. Ind. Appl. 1983, IA-19, 1098.
40. H. Wijshoff, Phys. Rep. 2010, 491, 77.
41. A. van der Bos, M.-J. van der Meulen, T. Driessen, M. van den Berg, H. Reinten, H. Wijshoff, M. Versluis, D. Lohse, Phys. Rev. Appl. 2014, 1, 014004.
42. J. Ando, H. Nomura, A. Kamiya, Microvasc. Res. 1987, 33, 62.
43. K. Yamamoto, T. Takahashi, T. Asahara, N. Ohura, T. Sokabe, A. Kamiya, J. Ando, J. Appl. Physiol. 2003, 95, 2081.
44. S. Kapur, D. J. Baylink, K.-H. William Lau, Bone 2003, 32, 241.
45. R. C. Riddle, A. F. Taylor, D. C. Genetos, H. J. Donahue, Am. J. Physiol. Cell Physiol. 2006, 290, C776.
46. N. Korin, M. Kanapathipillai, B. D. Matthews, M. Crescente, A. Brill, T. Mammoto, K. Ghosh, S. Jurek, S. A. Bencherif, D. Bhatta, A. U. Coskun, C. L. Feldman, D. D. Wagner, D. E. Ingber, Science 2012, 337, 738.
47. D. F. Duarte Campos, A. Blaeser, M. Weber, J. Jäkel, S. Neuss, W. Jahnen-Dechent, H. Fischer, Biofabrication 2013, 5, 015003.

48. D. F. Duarte Campos, A. Blaeser, A. Korsten, S. Neuss, J. Jäkel, M. Vogt, H. Fischer, Tissue Eng. Part A 2015, 21, 740.